Biol. Cybern. 83, 185–197 (2000)

Biological Cybernetics
© Springer-Verlag 2000

Wide-field, motion-sensitive neurons and matched filters for optic flow fields

Matthias O. Franz*, **Holger G. Krapp****

Max Planck Institute for Biological Cybernetics, Spemannstrasse 38, 72076 Tübingen, Germany

Received: 14 June 1999 / Accepted in revised form: 20 March 2000

Abstract. The receptive field organization of a class of visual interneurons in the fly brain (vertical system, or VS neurons) shows a striking similarity to certain self-motion-induced optic flow fields. The present study compares the measured motion sensitivities of the VS neurons (Krapp et al. 1998) to a matched filter model for optic flow fields generated by rotation or translation. The model minimizes the variance of the filter output caused by noise and distance variability between different scenes. To that end, prior knowledge about distance and self-motion statistics is incorporated in the form of a "world model". We show that a special case of the matched filter model is able to predict the local motion sensitivities observed in some VS neurons. This suggests that their receptive field organization enables the VS neurons to maintain a consistent output when the same type of self-motion occurs in different situations.

1 Introduction

While moving through the world, an animal experiences characteristic patterns of optic flow. These patterns are an important source of information about the animal's self-motion parameters, that is, the momentary translation and rotation. Before this information can be extracted, the optic flow has to be analyzed locally by elementary visual motion processing units. This causes several problems for the task of self-motion estimation:

1. Locally measured velocities depend on both the translatory and rotatory optic flow field. A single flow vector cannot be decomposed into its rotational and translatory components. This task requires the processing of at least seven flow vectors together (Longuet-Higgins and Prazdny 1980).
2. Translatory flow fields depend on the distance distribution of the visible objects. Therefore, the same translation in different scenes usually produces different flow fields.
3. Local image velocity measurements are affected by the noise in the visual input (Bouman et al. 1985) and in the synaptic signal transmission (Allen and Stevens 1994), as well as by the fact that biological motion detectors do not faithfully represent the local image velocity, due to their nonlinear and pattern-dependent response characteristics (Borst and Egelhaaf 1993).

A wide-field integration of selected velocity measurements can reduce the impact of these problems: by selecting only motion detectors that are consistent with a certain rotation or translation axis, a partial decomposition of the flow field is achieved because all flow components orthogonal to the selected ones do not contribute to the integrated signal. In addition, the integration of a large number of individual velocity measurements reduces noise, and – to a certain degree – the dependence on both the input pattern (Single and Borst 1998) and the distance distribution of the currently perceived scene. However, wide-field integration alone cannot solve the complete self-motion estimation problem: the integrated signal is still not specific for the selected self-motion axis because other self-motion types can also induce signals in the selected motion detectors. Moreover, a complete solution requires considering the distance dependence of the translatory flow (see, for example, the algorithms reviewed in Heeger and Jepson 1992), which is obscured by the integration process. But still, a selective wide-field integration might provide useful information on the global structure of the optic flow field, for instance, as input for a later self-motion estimation stage.

In the fly brain, the role of spatial integration is attributed to a class of wide-field, motion-sensitive neurons, the so-called tangential neurons in the lobula plate. Most of the previous studies suggested that these neu-

* *Present address*: DaimlerChrysler Research and Technology, P.O. Box 2360, 89013 Ulm, Germany

** *Present address*: Universität Bielefeld, Lehrstuhl Neurobiologie, P.O. Box 100131, 33501 Bielefeld, Germany

Correspondence to: M. O. Franz
(e-mail: matthias.franz@daimlerchrysler.com)

rons might be involved in the self-motion estimation process (review: Hausen and Egelhaaf 1989). Krapp and Hengstenberg (1996) have recently shown that the local motion sensitivities and preferred motion directions of a subgroup of the tangential neurons (vertical system, or VS neurons) closely resemble certain self-motion-induced flow fields. They argued that the VS neurons might act as a *matched filter* to sense self-motions (Krapp et al. 1998).

In the present study, we try to elucidate the functional role of the VS neurons by comparing their receptive field properties to a matched filter model for self-motion-induced flow fields. In its original sense, a matched filter is used to find matches between a template and an image by cross-correlating the image with a filter. It can be shown that, under certain assumptions, the best filter for this purpose is the template itself (matched filter theorem, Rosenfeld and Kak 1982; review of biological matched filters: Wehner 1987). The matched filter model proposed here is an extension of this idea from static images to optic flow fields. The model is designed to minimize the variance of the filter output caused by the various noise sources and the distance variability between different scenes. We show that a special case of the matched filter model is able to predict the local motion sensitivities of several VS neurons. This suggests that their receptive field organization minimizes the scene- and noise-dependent differences in their output whenever the same self-motion occurs. The model, however, does not reproduce the receptive fields of other VS neurons, indicating that further constraints are at work in their design.

In the following section, we briefly review the experimental findings obtained in electrophysiological studies on the tangential neurons. In Sect. 3, we develop a simple matched filter that we use to model the tangential neurons in Sect. 4. In Sect. 5, we compare the resulting weight sets to the local motion sensitivities of the VS neurons. We conclude by discussing the functional role of the VS neurons and relating our study to other approaches.

2 Processing of optic flow by wide-field neurons in the fly visual system

In the third visual processing area (lobula plate) of the fly, about 60 tangential neurons are known to respond in a directionally selective manner to wide-field motion stimuli (review: Hausen 1984, 1993; Hausen and Egelhaaf 1989). Tangential neurons integrate on their large dendrites the signals of many retinotopically arranged elementary movement detectors (EMDs; review: Reichardt 1987). At every tiny patch in the visual field retinal image shifts are analyzed by at least six EMDs whose preferred directions differ according to the arrangement of neighbouring ommatidia within the hexagonal lattice of the fly's compound eye, (Buchner 1976; Götz et al. 1979).

Two neuronal subsystems have been investigated more thoroughly, both of which are thought to be involved in gaze and flight stabilization: the horizontal system (HS; 1982a) and the vertical system (VS; Hengstenberg 1982; Hengstenberg et al. 1982). The three HS neurons mainly integrate the output of EMDs with horizontal preferred direction. In contrast, the VS neurons were long thought to receive input primarily from EMDs with vertical preferred direction, corresponding to the strong sensitivity to vertical downward motion within their receptive fields. Some hints that a few VS neurons also receive input from horizontally oriented EMDs (Hengstenberg 1981) led to a detailed investigation of the receptive field organization of the HS, VS and some other tangential neurons. The results of these investigations showed that most of these neurons are adapted to sense complex flow patterns rather than being sensitive to either horizontal or vertical motion only (Krapp and Hengstenberg 1996; Krapp et al. 1998).

During intracellular recordings from individual VS neurons, the local preferred directions (LPDs) and motion sensitivities (LMSs) were determined while a black dot rotated over a small area of the compound eye (Krapp and Hengstenberg 1997). When the instantaneous direction of dot motion coincided with the LPD, the measured response reached its maximum. An example of the measured response is shown in Fig. 1. As can be seen, the tangential neurons do not exclusively respond to image flow along their LPDs. The dependence of their output on the local stimulus direction is rather broad and reverses its sign (with respect to their resting activity) when the dot moves in the opposite direction of the LPD. This response directly reflects the directional properties of the EMDs (van Hateren 1990).

As an example, the distribution of LPDs and LMSs of VS7 is shown in Fig. 2. The distribution of LPDs in the VS7 response field is reminiscent of an optic flow

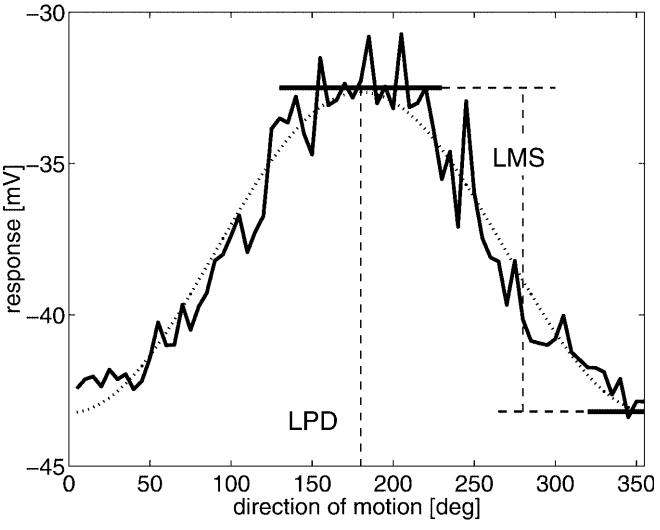

Fig. 1. Directional tuning curve of a vertical system (VS) neuron: the maximum occurs when the motion direction coincides with the local preferred direction (LPD), the minimum when the motion direction result is opposite to the LPD. The local motion sensitivity (LMS) is determined by the difference between the maximal and the minimal response (Krapp and Hengstenberg 1997). The *dotted line* depicts the scaled and shifted projection of the flow on a unit vector pointing into the LPD (cf. Sect. 3.1)

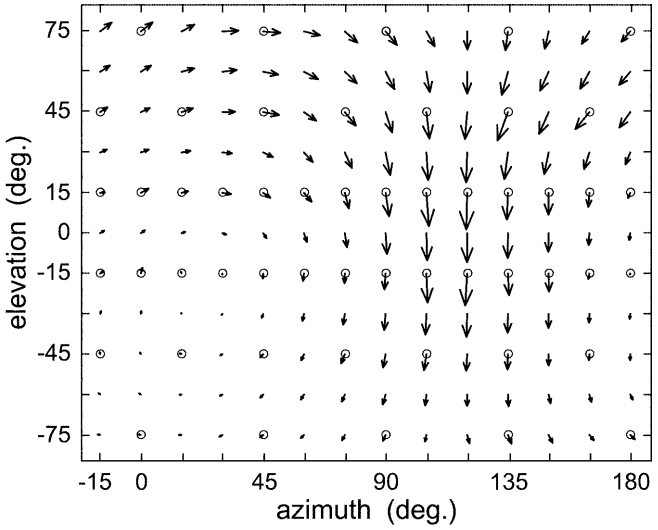

Fig. 2. Mercator map of the response field of the neuron VS7. The orientation of each arrow gives the local preferred direction, and its length denotes the relative motion sensitivity. Measurement positions are marked by small circles, arrows in between are interpolated (Krapp et al. 1998)

field generated by a rotation about an axis at an azimuth of about 30° and an elevation of about −15°. The LMSs show a pronounced anisotropy: (1) the LMSs near the rotation axis are generally smaller than those perpendicular to it; (2) the LMSs in the ventral part of the response field are smaller than those in the dorsal part. All VS neurons have these properties in common (Krapp et al. 1998). In addition, the response fields of most VS neurons do not make up the entire visual hemisphere but are confined to certain dorsal and medial regions only (cf. Fig. 7c).

Another wide-field neuron in the lobula plate, the so-called Hx neuron, belongs to neither the VS nor the HS. The neuron was found to have a response field most similar to a translatory optic flow field (Krapp et al. 1998). The LPDs of the Hx response field radially expand from a point at an azimuth of about 135° in the equatorial plane (cf. Fig. 7e). Although there is also an asymmetric sensitivity distribution, the Hx neuron responds more strongly to motion in the ventral than in the dorsal part of the visual field.

Can the distribution of the LMSs – in particular the dorsoventral asymmetry and the small LMSs near the self-motion axis – be understood from the properties of self-motion-induced optic flow? We will try to answer this question in the following sections by comparing the LMSs to a matched filter model for optic flow fields.

3 Matched filters for optic flow patterns

3.1 A matched filter model of a tangential neuron

Figure 1 shows that the local directional response characteristic of a tangential neuron can be modelled quite closely as the projection of the three-dimensional

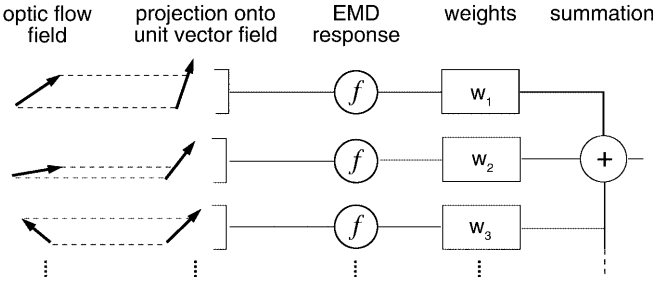

Fig. 3. Matched filter model: noisy optic flow vectors are projected onto a unit vector field corresponding to the LPDs. The projections are distorted by the response characteristic f of the EMD, weighted according to the LMS, and linearly integrated to give the filter output

flow vector $\mathbf{p}_i$ onto a unit vector $\mathbf{u}_i$. The vector $\mathbf{u}_i$ is tangential to the imaging surface and points into the LPD. Assuming a linear integration over the receptive field, the excitation e of a tangential neuron in response to a motion field can be described by the simplified model (cf. Fig. 3)

$$e = \sum_i w_i f(\mathbf{u}_i \cdot \mathbf{p}_i + n_i) \ , \qquad (1)$$

where $\cdot$ denotes the dot product. The functional dependence of the EMD output on the image velocity of the input is described by f, which is approximately linear for small velocities, reaches a flattened maximum at higher velocities, and then decreases again. We will discuss the modelling details of the EMD response below. The sum is taken over all EMDs in the receptive field at discrete locations with index i. The local weight w_i denotes the LMS, and n_i the noise in the locally measured motion signal. We assume the noise to be additive and isotropic.

What are the properties of such a processing element? The model produces its maximal output when the local flow vectors are parallel to the LPDs defined by the unit vector field. Similar to the matched filters in the image-processing literature (Rosenfeld and Kak 1982), the signal-to-noise ratio of the output is maximized when the directions of the local flow vectors coincide with the LPD template. This is obvious in (1), since in this case the dot product is maximal in relation to the local noise signal. We will call such a processing element a *matched filter* for optic flow patterns since it can be used to detect the presence of a particular directional pattern within the currently perceived optic flow.

3.2 Filters for self-motion-induced flow fields

The flow field depends on the layout of the visual system and of the environment. We model the visual system of the blowfly as a collection of EMDs arranged on the unit sphere. The viewing direction of an EMD (with index i) is described by a radial unit vector $\mathbf{d}_i$. When the fly translates with $\mathbf{T}$ while rotating with $\mathbf{R}$ about an axis through the origin, the self-motion-induced image flow $\mathbf{p}_i$ at $\mathbf{d}_i$ is given by

$$\mathbf{p}_i = -\mu_i(\mathbf{T} - (\mathbf{T}\cdot\mathbf{d}_i)\mathbf{d}_i) - \mathbf{R}\times\mathbf{d}_i \ , \qquad (2)$$

where the "nearness" $\mu_i = 1/D_i$ is the inverse distance D_i between the origin and the object seen in direction $\mathbf{d}_i$ (Koenderink and van Doorn 1987).

Equation (2) shows that the pattern of the local flow directions depends not only on the self-motion parameters, but also on the distances of the currently perceived environment. Thus, the repeated occurrence of a general flow field is a rather improbable event. There are, however, two exceptions: flow fields generated by either pure translation or pure rotation. In both cases, the local flow directions are independent of distance, which means that all flow fields generated by pure rotation about a common axis have the same local flow directions, as well as purely translatory flow fields with a common translation axis. In the following considerations, we will focus on these two cases as the most likely candidates affording the presence of a matched filter in the fly brain.

If we are interested in a rotatory flow field around an axis **a**, which we refer to as the *filter axis*, the LPD template has to be parallel to the local flow directions given by

$$\mathbf{u}_i^R = -\frac{\mathbf{R}\times\mathbf{d}_i}{\|\mathbf{R}\times\mathbf{d}_i\|} = -\frac{\mathbf{a}\times\mathbf{d}_i}{\sin\Theta_i} \qquad (3)$$

with Θ being the angle between viewing direction $\mathbf{d}_i$ and the filter axis **a**. Analogously, the LPD template for a translation along the axis **a** is

$$\mathbf{u}_i^T = -\frac{\mathbf{d}_i\times\mathbf{a}\times\mathbf{d}_i}{\sin\Theta_i} \ . \qquad (4)$$

Because of the broad directional response characteristic of the EMDs, such a filter will not respond selectively to self-motion along the filter axis but also to self-motion along other axes. The filter tuning therefore is only specific in the sense that, if the self-motion axis is varied, the largest response occurs when self-motion and filter axis coincide. The broadness of the response depends on the spatial arrangement of the viewing directions $\mathbf{d}_i$ and the weights w_i (cf. the detailed discussion in Dahmen et al. 1997). The filters are neither specific to pure rotation nor to pure translation since a rotatory filter responds to translation and vice versa. Again, the response is specific in the sense that it is maximal when filter type and self-motion type are the same.

Even when the self-motion parameters remain unchanged, the filter output will vary between different trials. Apart from the noise in the EMD output, this is due to the varying distance distribution of the current scene, which affects the translatory flow. The variance of the filter signal can be minimized by choosing an appropriate set of local weights. EMD signals with high noise content and viewing directions with high distance variability should receive less weight, if a stable filter output is desired. We will describe in Sect. 3.4 how to design an optimal weight set that minimizes the variance of the filter output as long as the self-motion parameters do not change.

3.3 Modelling the EMD response

The steady state response of a tangential neuron to different angular velocities is thought to reflect the functional dependence of the fly EMD on pattern velocity (shown in Fig. 4). For small velocities (0–10°/s), the EMD signal is approximately linear with velocity, until it reaches a plateau-like maximum in the range of about 20–200°/s (Egelhaaf and Borst 1993). At higher velocities, the EMD signal decreases again owing to the intrinsic characteristics of a correlation-type EMD (Reichardt and Varjú 1959).

Instead of modeling the EMD response in one function, we consider here two limit cases that will allow us to derive analytic solutions for the optimal weight set. To keep the model simple, we do not consider the dependence of the EMD output on contrast and spatial frequency of the input pattern.

Linear range model. The linear range can be modelled quite easily by using the identity function for f so that (1) becomes

$$e = \sum_i w_i(\mathbf{u}_i\cdot\mathbf{p}_i + n_i) \ . \qquad (5)$$

Since this model uses the linear range of the EMDs, its output can encode the relative value of the self-motion parameter along its axis: the faster the translation or rotation of interest, the larger are the flow vectors, and, as a consequence, the larger is the filter output [cf. (5)]. However, such a filter responds also to flow fields generated by rotation or translation along other axes (cf. Sect. 3.2). To arrive at an estimate of the true self-motion component, these components have to be removed at later processing stages (Franz et al. 1999).

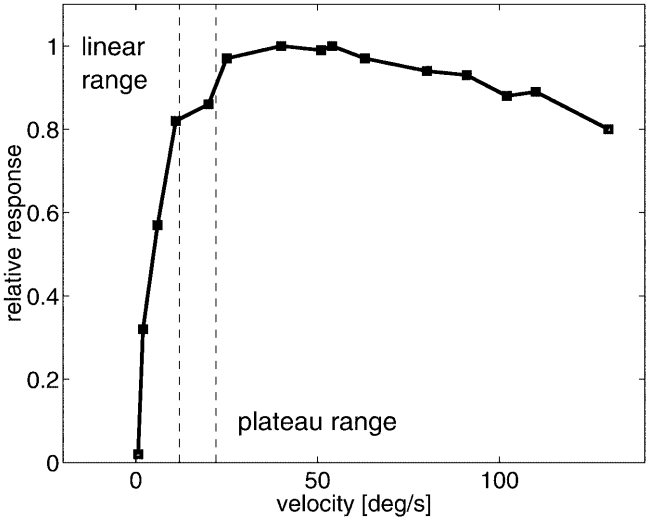

Fig. 4. Steady state response of the tangential neuron HSE to a grating moving at different velocities. Two limit cases are modelled: the linear range at smaller velocities and the relatively constant range around the maximal response (redrawn after Hausen 1982b)

Plateau range model. The plateau around the maximum can be modelled by dividing the current detector input by the absolute value of the local flow projection $|\mathbf{u}_i \cdot \mathbf{p}_i|$, which might be obtained from an averaging process over a small time scale. When the local flow projection is below some threshold P, we set the detector output to 0. The resulting EMD signals above the threshold are "equalized" to an average value of 1 for all velocities. Using this EMD model, we obtain the filter output

$$e = \sum_{|\mathbf{u}_i \cdot \mathbf{p}_i + n_i| > P} w_i \frac{\mathbf{u}_i \cdot \mathbf{p}_i + n_i}{|\mathbf{u}_i \cdot \mathbf{p}_i|} \quad . \tag{6}$$

Note that this model is still specific to the self-motion along the filter axis since the percentage of "activated" EMDs will be highest when the current flow pattern and the LPD template coincide. In contrast to the linear range model, the plateau range model allows us to detect only the sign of the self-motion along the filter axis, not its relative value. In this case, a larger filter output indicates a higher probability that the preferred flow pattern occurred. Again, the filter output does not encode the true self-motion axis since it responds also to other self-motions.

In both models, it is desirable to keep the variance of the filter output caused by noise and distance variability as small as possible. This requirement leads to different optimal weight sets for the two models that are derived in the next section.

3.4 Minimization of filter output variance

Even when the self-motion parameters remain exactly the same, the output of our matched filter model will vary from trial to trial due to the noise in EMD signals and the varying distances of the currently perceived scene. In our model in (1), all the different noise sources are combined into a common additive noise component n_i with standard deviation Δn_i and zero mean. Among the possible sources of error are photon noise in the visual input, synaptic transmission noise, and the characteristics of the elementary motion detectors such as their limited aperture and the dependence of their output on contrast frequency and image contrast. Although the nature of these error sources is quite different, they all lead to deviations of the measured flow component from the real one.

In addition to noise, the second cause of variable filter output is the distance variability between different scenes. We express this fact as a scattering of the nearnesses around their average value $\langle \mu_i \rangle$ over all scenes. To facilitate the mathematical analysis, we have to assume that the nearness variations at different points in the visual field are statistically independent. This would be ideally true in an environment consisting of small point-like objects.

Based on these assumptions, we can find expressions for both models describing the variance of the filter output caused by noise and distance variability. By choosing the appropriate weight sets, this variance can be minimized using the standard Euler–Lagrange formalism (details about the derivation can be found in the Appendix). The resulting weight set for the linear range model is given by

$$w_i^R = N \frac{\sin \Theta_i}{\Delta t_i^2 + \Delta n_i^2} \tag{7}$$

$$w_i^T = N \frac{\langle \mu_i \rangle \sin \Theta_i}{\Delta t_i^2 + \Delta n_i^2} \tag{8}$$

where the w_i^R and w_i^T are the optimal weights for a rotatory and a translatory filter, respectively. N is a normalization factor and $\langle\rangle$ denotes the average over all trials. The variance Δt_i^2 of the translatory flow projection depends on the distribution of the translation speed and direction, and on the distance distribution of the viewing direction $\mathbf{d}_i$. Δt_i^2 is especially high in viewing directions with small absolute distance, high distance variability, and a large component of the translation vector along $\mathbf{u}_i$ [cf. 2].

The corresponding weight set for the plateau range model is

$$w_i^R = N \frac{\sin^2 \Theta_i + t_i^2}{\Delta t_i^2 + \Delta n_i^2} \tag{9}$$

$$w_i^T = N \frac{\langle \mu_i^2 \rangle \sin^2 \Theta_i + r_i^2}{\Delta t_i^2 + \Delta n_i^2} \quad . \tag{10}$$

Here t_i^2 is the mean square translatory proportion of the flow projection while rotating about the filter axis, r_i^2 the mean square rotatory proportion while translating along the filter axis. These terms arise from the normalization factor $1/(\mathbf{u}_i \cdot \mathbf{p}_i)$ in (6), which amplifies not only smaller local flow signals but also the corrupting factors noise and variability of the translatory flow. When the average flow (which includes t_i and r_i) is large, the amplification of the corrupting factors is small. Thus, the corresponding EMD signal receives a higher weight in the optimal solution.

As can be seen from the above equations, the optimal solution for both models assigns the weights according to the local variance of the corrupting factors noise and variability of the translatory flow. Flow projections with high noise content and large variation of the translatory component receive less weight since they contribute strongly to the variance of the filter output. The denominators in all weight sets are identical; only the functional dependence on $\sin \Theta$ and the additional terms t_i^2 and r_i^2 lead to differences between the linear range and the plateau range model.

The actual computation of the weight sets requires prior knowledge about the distance statistics of the habitat, the self-motion statistics, and the EMD noise Δn_i^2. Since all of these parameters are currently unknown for the fly, we either have to provide crude estimates or treat them as free parameters that have to be fitted to the data. In the next section, we describe a mixed approach based on a simplified "world model" that yields a low-dimensional parameterization of the weight sets.

4 Modelling of tangential neurons

4.1 Distance statistics

The variance of the translatory flow projection is approximately given by [cf. (A5) in the Appendix]

$$\Delta t_i^2 \approx \frac{\Delta D_i^2}{\langle D_i \rangle^4} \langle T_i^2 \rangle \tag{11}$$

where ΔD_i^2 and $\langle D_i \rangle$ denote the variance and mean of the distance $D_i = 1/\mu_i$ at the viewing direction $\mathbf{d}_i$, and $\langle T_i^2 \rangle$ the average square projection of $\mathbf{T}$ on the LPD $\mathbf{u}_i$. A concise statistical description of the flight patterns of the blowfly and its habitat is still not available in the literature, but we can make some guesses of how the probability distribution of the distances might look. If we assume that the animal usually flies at heights below 2 m, it is likely that, on the average, objects seen at lower elevations in the visual field will have a smaller distance than objects near or above the horizon. We model the average distance $\langle D \rangle$ experienced during horizontal flight by

$$\langle D \rangle = \begin{cases} D_0 & : \epsilon \geq 0 \\ \frac{\beta D_0}{\sqrt{1+(\beta^2-1)\cos^2\epsilon}} & : \epsilon < 0 \end{cases}, \tag{12}$$

where D_0 denotes a typical distance, ϵ the elevation of the viewing direction and $\beta = h/D_0$ the ratio of the average flight altitude h and D_0. The variance of the distances ΔD^2 is chosen to be the same in all viewing directions. The resulting geometry of the distance model is that of a sphere that is flattened in the lower part of the visual field (see Fig. 5a). This model is clearly a gross simplification of the real-world situation, but for our purpose it is sufficient insofar as it provides a basic dorsoventral asymmetry.

4.2 Flight statistics

To estimate $\langle T_i^2 \rangle$ and t_i^2, we assume a unimodal distribution for the translation direction

$$p(\alpha_T, \epsilon_T) = N_{vM} \exp(\kappa_1 \cos\alpha_T + \kappa_2 \cos\epsilon_T) \tag{13}$$

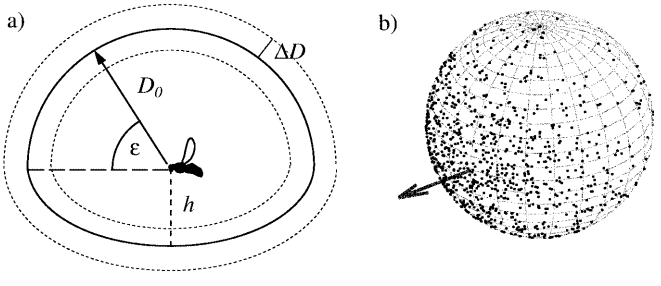

Fig. 5. Simplified "world model" of a blowfly flying at an average height h over ground. **a** Anisotropic distribution of the average distances in the visual field. The distance deviation ΔD is assumed to be independent of the viewing direction. **b** one thousand samples generated by the two-dimensional von Mises distribution of the translation directions. The *arrow* indicates the maximum of the distribution that is in the forward direction

around the forward direction, where N_{vM} is a normalization factor and α_T and ϵ_T indicate the azimuth and the elevation of the translation direction. This distribution is a three-dimensional analogue of the von Mises distribution (Batschelet 1981). The directional concentration of the distribution are determined by κ_1 and κ_2: smaller values lead to a broader directional distribution. In this study, we choose $\kappa_1 = 2.0$ and $\kappa_2 = 4.0$ so that the distribution becomes broader in the horizontal than in the vertical direction (see Fig. 5b). The exact choice of the distribution is not critical for the results presented in Sect. 5, as long as it is unimodal and sufficiently broad. We tested several similar distributions with no significant effect on the results. Additionally, we assume that the absolute value of $\mathbf{T}$ is distributed independently of its direction with a mean value T. The $\langle T_i^2 \rangle$ in (11) are then given by $T^2 \langle p_i^2 \rangle$ with the expectation $\langle p_i^2 \rangle$ of the square projection of the translation direction on the unit vector $\mathbf{u}_i$.

We assume rotation to be independent of translation, and uniformly distributed. As a consequence, r_i^2 is constant over the visual field. These assumptions do not always hold in the real fly, since some translatory motions may be coupled to rotations (Schilstra and van Hateren 1998), or some rotation axes might be more frequent than others. For our modeling purposes, however, only rough estimates are needed.

4.3 Parameterization of weight sets

The normalized distance model $\hat{D}_i = \langle D_i \rangle / D_0$ from (12), a uniform ΔD^2 over the visual field, and the distribution of flight directions allow us to compute the terms requiring prior knowledge in the weight sets. Assuming a uniform noise variance Δn^2 over the visual field, the optimal weight sets (7) and (8) of the linear range model can be expressed as

$$w_i^R = \frac{N \sin\Theta_i}{1 + \zeta \frac{\langle p_i^2 \rangle}{\hat{D}_i^4}} \tag{14}$$

$$w_i^T = \frac{N \sin\Theta_i / \hat{D}_i}{1 + \zeta \frac{\langle p_i^2 \rangle}{\hat{D}_i^4}} \quad . \tag{15}$$

with the parameter $\zeta = \Delta D^2 T^2 / \Delta n^2 D_0^4$. For the plateau range model, this leads to the parameterized weight sets

$$w_i^R = N \frac{\sin^2\Theta_i + \langle p_i^2 \rangle v_R}{1 + \zeta \frac{\langle p_i^2 \rangle}{\hat{D}_i^4}} \tag{16}$$

$$w_i^T = N \frac{\sin^2\Theta_i / \hat{D}_i^2 + v_T}{1 + \zeta \frac{\langle p_i^2 \rangle}{\hat{D}_i^4}} \tag{17}$$

where $v_R = T^2 / (D_0^2 \langle R^{\parallel 2} \rangle)$ and $v_T = r_i / \langle T^{\parallel 2} \rangle$ [cf. (A19) and (A20) in the Appendix]. The $\langle p_i^2 \rangle$ are computed from

1,000 direction samples generated by the von Mises distribution.

The resulting weight sets (14) and (15) for the linear range model depend only on four free parameters: the degree of dorsoventral asymmetry β [cf. (12)], ζ, and the direction of the filter axis (with azimuth α and elevation ϵ). The weight sets (16) and (17) of the plateau model include an additional fifth parameter v. These weight sets were fitted to the LMSs measured by Krapp et al. (1998) using their mean values and standard deviations. The fitting was done by evaluating the χ^2 value for a given parameter set using the standard deviation of the measurements. The parameter values were varied until a global minimum was reached. The step size of the parameters was 0.1 for β, ζ, and v, and 1° for the angular coordinates of the sensor axis. From the 52 LMS measurement positions, the one at −15° elevation and 180° azimuth had to be discarded since the fly's body occluded part of the visual stimulus. Goodness of fit was tested using a χ^2 distribution with 47 *df* for the linear range model, and 46 for the plateau range model. Theoretical weight distributions with a significance $p < 0.05$ were rejected.

5 Results

Provided that the world model captures some essential properties of the fly's environment, the procedure described above allows us to test two hypotheses: are the VS neurons matched filters optimized (1) for the linear range, or (2) for the plateau range of the EMDs? The results with $p \geq 0.0001$ are summarized in Table 1.

The first hypothesis could be rejected for all VS neurons with high probability. None of the weight sets computed according to (14) produced a fit with $p > 0.004$ (VS4) to the measured data. We conclude from this result that the linear range model cannot explain the observed LMSs of the VS neurons.

Table 1. Results of the fitting procedure with $p \geq 0.0001$ for single VS neurons. α and ε denote azimuth and elevation of the sensor axis, α' and ε' the axes estimated by Krapp et al. (1998). The table shows results for the plateau range model (16) and the linear range model (14). All weight sets with $p < 0.05$ are rejected

	χ^2	p	β	ζ	v	α	ε	α'	ε'
(16)									
VS4	30.8	0.96	0.4	0.9	0.1	26°	−4°	29°	−7°
VS5	52.1	0.25	0.5	2.3	0.5	14°	2°	10°	−2°
VS6	57.6	0.12	0.5	2.3	0.2	5°	−4°	0°	3°
VS8	75.3	0.004	0.5	1.8	0.6	−37°	−9°	−51°	9°
VS9	86.6	0.0003	0.5	1.4	0.4	−40°	−1°	−60°	12°
(14)									
VS4	76.7	0.004	0.40	0.9	–	21°	−5°	29°	−7°
VS8	85.3	0.0003	0.50	1.1	–	−37°	−8°	−51°	9°

The second hypothesis cannot be rejected for VS4, VS5, and VS6. The plateau range model accurately predicts the LMSs of these neurons, as the low χ^2 values indicate. This suggests that VS4–VS6 can be understood as matched filters that are optimally designed for detecting self-motion-induced flow patterns in the plateau range of the EMDs.

The second hypothesis does not hold for VS1–VS3 and VS7–VS10. This means that the plateau range model cannot predict the LMSs of these neurons correctly.

Interestingly, the degree of dorsoventral asymmetry β is almost the same in all results, which makes this feature of the internal world model highly reproducible. The differences in ζ and v arise mainly because of the ad hoc chosen von Mises distribution, which affects $\langle p_i^2 \rangle$. Although we did not fit the parameters κ_1 and κ_2 to the measurements, variations in these parameters did not lead to qualitative changes in the computed weight distributions. The obtained filter axes of VS4–VS6 correspond closely to those estimated by Krapp et al. (1998).

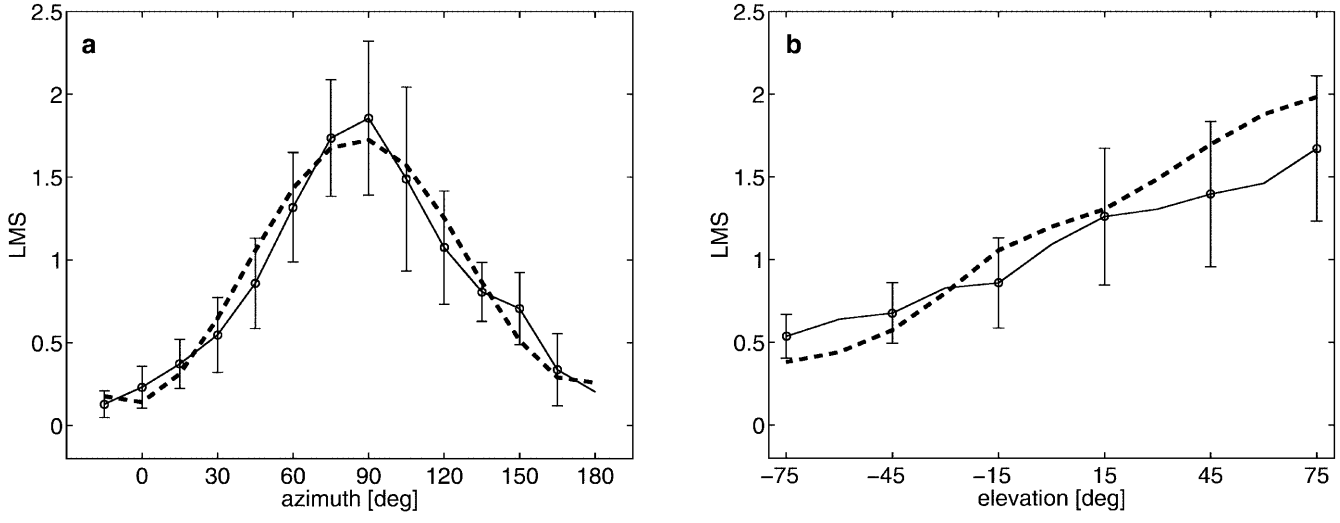

Fig. 6. **a** Horizontal section at −15° elevation through measured LMSs (*circles*) and weights predicted by the plateau range model (*dashed line*) for VS6. **b** Vertical section at 45° azimuth through measured (*circles*) and predicted data (*dashed line*) for VS6

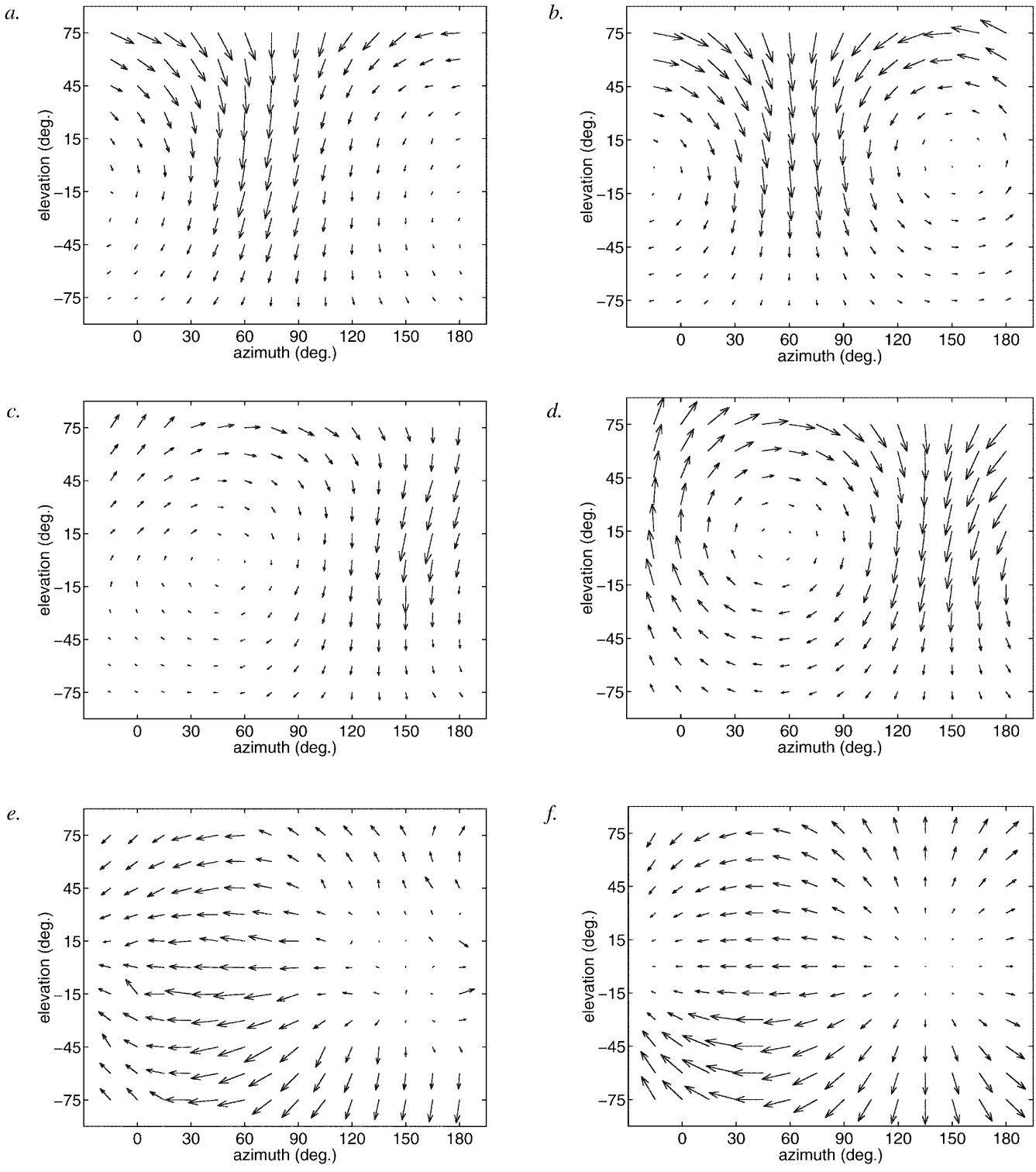

Fig. 7. a Averaged response field of VS4 from five animals. **b** Theoretical response field obtained by fitting (16). **c** Averaged response field of VS10 from five animals. This neuron responds only weakly to motion in the frontal area. **d** Theoretical response field obtained by fitting (16). **e** Measured response field of a single Hx neuron. **f** Theoretical response field obtained from (17) by assuming a constant standard deviation (notation as in Fig. 1)

A closer look at the measured sensitivities shows that the main difference between the tested alternative weight sets lies in the different angular dependences: equation (16) predicts a $\sin^2\Theta$ dependence, whereas (14) predicts a $\sin\Theta$ dependence. The horizontal section at $-15°$ (Fig. 6a) for VS6 illustrates that the measured LMSs, LMbs follow very closely a $\sin^2\Theta$ curve so that a $\sin\Theta$ curve would lead to large deviations.

The qualitative features of the LMS distribution of VS4 (Fig. 7a,b), VS5, and VS6 can be interpreted from

(16): the ventral retinal regions are less weighted because of the less predictable influence of the translatory flow field. This is due to the shorter distances in the ventral part of the distance model that increase Δt in (11). Flow regions around the rotation axis receive less weight as well, since the rotatory flow signal is small relative to the sensor noise and Δt. While the horizontal LMS distribution is reproduced very closely (Fig. 6a), most of the discrepancies between theory and data occur at the highest and lowest elevations (cf. Fig. 6b). As our theoretical world model is very crude, this could probably be corrected by using a more sophisticated world model. Figure 7 demonstrates also that the LPDs of the neurons agree well with the predicted directions from (3) and (4), but the statistical significance remains to be tested.

Why does the plateau range model not reproduce the LMSs of the other VS neurons? Figure 7c shows that VS10 (and also VS7–VS9) is only weakly sensitive to motion in the frontal visual field whereas the plateau range model predicts a high frontal sensitivity (cf. Fig. 7d). This property cannot be explained by an optimality criterion based on self-motion estimation and might be due to anatomical or physiological factors. Figure 7 suggests that the plateau range model could reproduce the LMSs in the motion-sensitive areas of their visual field, but, as we have no clear description of their extent, we cannot corroborate this claim by a statistical analysis. Similar considerations apply to VS1–VS3, which are almost insensitive to motion in most of the caudal hemisphere.

To test our predictions for translatory filters, we compared the translatory weight sets (15) and (17) to the measured LMSs of the Hx neuron (Fig. 7c, Krapp et al. 1998). Since we presently have only one data set of the Hx neuron, we could not apply the same statistical procedure. As a plausibility test, we assumed a constant measurement error over the visual field and used again the same fitting procedure for (15) and (17). Both weight distributions succeeded in reproducing the elevational dependence, but the azimuthal weight distribution is again better described by the $\sin^2\theta$ dependence in (17). The asymmetry of the receptive field organization is reversed with respect to the filters for rotatory flow fields, so that ventral retinal regions receive more weight than dorsal regions (Fig. 7e,f). This can be interpreted from our theory: in the ventral part of the visual field, the variability of the translatory flow is higher, but at the same time the signal-to-noise ratio is better because of the larger flow vectors. For the distance statistics we consider here, the better signal-to-noise ratio is more important, so that the ventral regions receive higher weights.

6 Discussion

6.1 Summary

The local motion sensitivities of VS4, VS5, and VS6 can be accurately predicted by a matched filter model that minimizes the variance of the filter output caused by noise and the distance-dependent variability of the translatory flow. This requirement explains the observed dorsoventral asymmetry of the VS neurons: Since the average distance in the ventral visual field is smaller, the relative distance variability is higher, which in turn leads to a higher variability of the translatory flow field. Thus, the ventral regions contribute more to the variance of the filter output, which results in a smaller weight. Although not statistically shown, the theory can also reproduce the reversal of the asymmetry in the translatory Hx neuron. Here, the higher signal-to-noise ratio of the ventral flow outweighs the detrimental effect of its variability so that the ventral regions receive a higher weight.

The matched filter takes as input local motion detectors operating in the plateau range. The output of such a filter indicates the presence and the rotation direction of the flow field about its filter axis but is not proportional to the rotation rate. An alternative model operating in the linear range of the motion detectors is capable of directly encoding the rotation rate but could be rejected with high probability. We conclude that the VS neurons are not optimized for directly encoding rotation rates in their output. The results on VS4–6 suggest that they rather act as robust detectors for rotatory flow fields about a set of selected axes.

The matched filter model failed to explain the LMS distribution of VS1–VS3 and of VS7–VS10. The receptive fields of these neurons are very close to the model in some regions, but in other regions they show only weak LMSs where the model predicts a high motion sensitivity. This indicates that further, possibly anatomical or developmental, constraints are at work in their design.

6.2 The functional role of VS neurons

In Sect. 3.2, we noted that a matched filter alone cannot extract the true self-motion component along its filter axis since it also responds to self-motion along other axes. The VS neurons, for instance, not only respond to horizontal rotation but also – to a lesser degree – to lift translations (Krapp et al. 1998). Moreover, the wide-field integration averages over all local distance dependences of the translatory flow thereby neglecting the information contained in local distance variations (*motion parallax*). Most approaches in the computer vision literature to self-motion estimation (see overviews in Heeger and Jepson 1992; Lappe et al. 1999) either explicitly (e.g. Rieger and Lawton 1985; Hildreth 1992) or implicitly (e.g. Heeger and Jepson 1992; Lappe and Rauschecker 1993) use motion parallax to decompose the flow field into its rotational and translational components. In contrast to these approaches, our matched filters are explicitly designed to suppress the effects of motion parallax to maintain a consistent output. This, however, can only be achieved as long as the distance statistics do not deviate too much from those used for the filter design. An approach solely based on wide-field integration therefore has to be confined to a certain domain: it provides no general solution to the

self-motion estimation problem. Our results on VS4–VS6 suggest a further restriction: the VS neurons seem to be optimized for operating in the plateau range of the EMDs. In this range, the VS neurons can only encode the sign of the rotatory flow about their axis, not its apparent rotation rate.

What is the functional role of the VS neurons, after all these restrictions? Robot experiments have shown that the linear range model can be used to estimate self-motion in indoor environments by a suitable linear combination of matched filter outputs (Franz et al. 1999). A similar idea might apply to the plateau range model: a later integration stage could interpolate between the responses of the single VS neurons that together would form a population code for the current rotation axis and direction. This information should be sufficient for flight or gaze control since the animal, in a normal behavioural situation, operates under closed-loop conditions (Warzecha and Egelhaaf 1998). A suitable combination with other matched filters could also lead to signals that are more specific to one type of self-motion: for instance, the inhibitory interaction of a hypothetical translatory "lift" neuron could be used to correct the responses of the VS neurons to lift translations. Finally, an integration stage could also explain the "gaps" in the receptive fields of the VS1–VS3 and VS7–VS10. If some VS neurons responded together as an ensemble, they could mutually fill in their "gaps". For example, VS10 shows almost no motion sensitivity in the frontal visual field (Fig. 7c) whereas VS3 responds strongly in this area (Krapp et al. 1998). Together, they could form an optimal matched filter at a later integration stage if the signal of one of them was reversed.

Thus, a complete characterization of the functional role of the VS neurons requires further research: first, the validity and the scope of the plateau range model for self-motion estimation needs to be established in simulations or robot experiments. Second, anatomical and physiological investigations have to clarify how the output of these neurons is processed and integrated at later stages.

6.3 Model assumptions and approximations

EMD model. Our matched filter model considers only the directional dependence and part of the velocity characteristic of the Reichardt detector. It is well known that the output of biological EMDs depends on the contrast and the contrast frequency of the input pattern, that is, the ratio of the velocity over the spatial frequency of the pattern (Reichardt 1987). This does not necessarily reduce the performance of a system based on biological EMDs, though. Warzecha and Egelhaaf (1998) showed recently that the performance of the blowfly in optomotor tasks comes close to that of a hypothetical observer using perfect velocity sensors.

From the modelling point of view, inhomogeneous distributions of contrast and spatial frequencies in the animal's environment could be included in the optimization. For instance, a smaller weight could be assigned to viewing directions where low contrasts are to be expected since this leads to less reliable motion estimates. A systematic investigation of natural environments could help to clarify whether animals utilize possible anisotropies of the contrast distribution of their habitat.

For mathematical convenience, we had to limit our study to the linear and the plateau range of the EMD steady state response. We did not take into account dynamical effects such as transients in the EMD output or adaptation processes. Although it is not clear how dynamical factors affect the filter performance, the model includes two properties that might help to keep the filter output stable: first, wide-field spatial integration reduces the influence of transient EMD output (Borst and Egelhaaf 1993); second, the matched filters are designed to minimize the variance of the filter output between trials.

Distance model. Some of the remaining discrepancies between theory and data can be attributed to the crude distance model. Although more sophisticated world models might lead to a better correspondence, they do not necessarily provide more insights, as the asymmetry of our simple distance model already suffices to reproduce the dorsoventral asymmetry of the measured sensitivities. A more realistic world model certainly would have to be modified, for example, by permitting a variable distance deviation over the visual field, or by including azimuthal variations of the average distances. It is quite probable, for instance, that the average frontal distances are larger than the lateral distances, since the insect, if not landing, tends to fly in the open space between obstacles.

While similar distance models might apply to other flying animals, the distance distribution should look different in walking animals. In contrast to that of flying animals, the distance of the visual system to the ground remains relatively constant during locomotion so that the distance variability is small in the ventral visual field. We expect therefore that the dorsoventral asymmetry of rotatory neurons is less pronounced in walking animals, but it should be still observable in the special case of an essentially flat environment. A hint in that direction could be the fact that some crab species inhabiting mud flats respond more strongly to optokinetic stimulation near and above the horizon (Nalbach and Nalbach 1987). As with flies, the decisive factor could be the large distances near and above the horizon that keep the translatory flow component too small to interfere.

Flight statistics. We did not fit the von Mises distribution to the measured data. This primarily affects the consistency of the parameters ζ and v between different neurons. An appropriate choice of the translation statistics might lead to more consistent values among the data sets, but this would require a concise statistical description of the blowfly's flight trajectories, which is currently not available in the literature. However, the exact form of the distribution turned out to be unimportant for the results as long as it was unimodal

and sufficiently broad. Qualitative differences arise when the translation distribution becomes sharply peaked as, for instance, in an animal that translates only in the forward direction. In this case, the translatory component almost vanishes in a rotatory filter tuned to roll movements (such as VS6). As a consequence, distance-dependent asymmetries should be hardly observable in such a filter.

6.4 Relation to other matched filter approaches

Dahmen et al. (1997) derived a matched filter as a special case of the iterative algorithm by Koenderink and van Doorn (1987). Similar to many self-motion estimation algorithms (starting with Bruss and Horn in 1983) including our approach, this algorithm is derived from a least-square principle. Instead of minimizing the variance of the filter output, Koenderink and van Doorn minimize the difference of the measured flow field to a flow field derived from the self-motion estimates. In contrast to ours, their approach assumes no prior knowledge about distance statistics.

Assuming a spherical environment, Dahmen et al. (1997) showed that the first iteration of the algorithm of Koenderink and van Doorn can be implemented by a matched filter similar to our linear range model. Dahmen et al. tested their filter using simulated noisy flow as input. They report excellent performance in spherical environments, in many cases close to that of the iterative algorithm. However, the matched filter of Dahmen et al. was derived for a homogeneous distance distribution and thus cannot explain the dorsoventral asymmetry of the VS neurons.

The weights of their matched filter can also be derived from the linear range models (7) and (8) by assuming constant average distance, distance deviation, and noise over the visual field. This suggests that the linear range model can be understood as an extension of the approach of Koenderink and van Doorn (1987) to cases where prior knowledge about distance statistics is available. As a consequence, our results on the linear range model apply also to the matched filter model of Dahmen et al. (1997). In particular, their model produces the same angular dependence as the linear range model that could be rejected for the VS neurons with high probability.

Perrone (1992) presented a matched filter model of self-motion estimation in the primate visual cortex. In his approach, the motion field was sampled at each image position by several sensors tuned to different velocity vectors. Perrone's matched filters use only those velocity signals as input that are consistent with a given set of self-motion parameters and distances. Instead of weighting the sensor according to an optimality criterion, his filter chooses the most active velocity sensor at each image position. These properties make Perrone's model less suitable for being applied to the VS neurons since no evidence of a parallel system of EMDs with different velocity tuning has been found in the fly. Since the self-motion estimate is derived from the most active filter using a winner-takes-all strategy, every combination of self-motion parameters and distances needs its own matched filter. The number of filters can be somewhat reduced by constructing only filters for the most probable parameter sets, for example, by considering only fixating eye movements (Perrone and Stone 1994). But still this approach would require a number of matched filters well beyond the 60 tangential neurons of the fly "to avoid" that self-motion directions between the filter axes "are" misrepresented.

6.5 Conclusion

In the present study, we compared the receptive field properties of the VS neurons to a matched filter model. The comparison showed that some of the VS neurons are optimized for detecting the sign of rotatory flow fields about selected axes, but none of them for directly encoding rotation speeds. Our results indicate that a further understanding of the functional role of the tangential neurons requires research efforts at three different levels: first, theoretical studies on how the plateau model can be used to estimate self-motion, second, an investigation on how the output of the tangential neurons is integrated at later processing stages, and third, a characterization of the fly's environment in terms of the distance statistics, flight patterns, and the distribution of visual structures.

Acknowledgements. The authors wish to thank R. Hengstenberg, H.A. Mallot, M. Egelhaaf, H. Dahmen, M.V. Srinivasan, and J. Zeil for helpful comments on the manuscript. Financial support to M.O.F. was provided by the Human Frontier Science Program, and to H.G.K. by the Max-Planck-Gesellschaft and the Deutsche Forschungsgemeinschaft.

Appendix. Derivation of the optimal weight sets

A.1 Variance of the filter output

The distance variability affects only the translatory flow field. From (2) and (5), the translatory part of the flow projection is given by

$$-\mu_i(\mathbf{T} - (\mathbf{T}\cdot\mathbf{d}_i)\mathbf{d}_i)\cdot\mathbf{u}_i = -\mu_i T_i \tag{A1}$$

with $T_i = \mathbf{T}\cdot\mathbf{u}_i$. The same self-motion in a different environment results in a local flow projection differing from the previous one by

$$\Delta\mu_i T_i + n_i \tag{A2}$$

because of the local noise signal n_i and the different nearness $\mu_i + \Delta\mu_i$ at $\mathbf{d}_i$.

In the linear range model, this leads to the variance of the filter output Δe^2 [cf. (5) and (A2)]

$$\Delta e^2 = \left\langle \left(\sum_i w_i(\Delta\mu_i T_i + n_i) \right)^2 \right\rangle \tag{A3}$$

where the $\langle\rangle$ denote the expectation over all trials. As n_i and μ_i are assumed to be statistically independent, this expression simplifies to

$$\Delta e^2 = \sum_i w_i^2 (\Delta t_i^2 + \Delta n_i^2) \tag{A4}$$

with Δt_i^2 being the variance of the translatory flow projection

$$\Delta t_i^2 = \Delta \mu_i^2 \langle T_i^2 \rangle . \tag{A5}$$

Analogously to the linear range model, the variance of the filter output in the plateau range model is given by [cf. (6) and (A2)]

$$\Delta e^2 = \sum_i w_i^2 \frac{\Delta t_i^2 + \Delta n_i^2}{\langle (\mathbf{u}_i \cdot \mathbf{p}_i)^2 \rangle} \ . \tag{A6}$$

For our model in Sect. 4, we approximate μ_i as

$$\mu_i = \frac{1}{D_i} \approx \frac{1}{\langle D_i \rangle} - \frac{D_i - \langle D_i \rangle}{\langle D_i \rangle^2} \tag{A7}$$

with the distance D_i, so that the variance of the translatory flow becomes

$$\Delta t_i^2 \approx \frac{\Delta D_i^2}{\langle D_i \rangle^4} \langle T_i^2 \rangle \ . \tag{A8}$$

A.2 Optimal weights

The optimal weight set is chosen such that the variance Δe^2 of the filter signal is minimized. To find a unique solution, we have to impose further constraints. For the linear range model, we stipulate that the average filter signal should be equal to the self-motion component along its filter axis. In the case of a rotatory filter, the filter output due to rotation component $\mathbf{R}^{\parallel}$ (with absolute value $\|\mathbf{R}^{\parallel}\| = R^{\parallel}$) along the filter axis is given by [cf. (2)]

$$\sum_i w_i \mathbf{d}_i \times \mathbf{R}^{\parallel} \cdot \mathbf{u}_i = R^{\parallel} \sum_i w_i \sin \Theta_i \ . \tag{A9}$$

This leads to the condition

$$R^{\parallel} \sum_i w_i \sin \Theta_i = R^{\parallel} \ , \tag{A10}$$

which is equivalent to

$$\sum_i w_i \sin \Theta_i = 1 \ . \tag{A11}$$

The optimal weight set can now be derived from the Euler–Lagrange equation

$$\frac{\partial}{\partial w_i} \left(\Delta e^2 - \lambda \left(\sum_i w_i \sin \Theta_i - 1 \right) \right) = 0 \ , \tag{A12}$$

with a Lagrange multiplier λ. This finally leads to the analytic expression for the optimal weight set w_i^R of a rotatory filter

$$w_i^R = N_R \frac{\sin \Theta_i}{\Delta t_i^2 + \Delta n_i^2} \tag{A13}$$

with a suitable normalization factor N_R such that $\sum_i w_i \sin \Theta_i = 1$.

In an analogous procedure, we obtain the condition for a translatory filter

$$\sum_i w_i \langle \mu_i \rangle \sin \Theta_i = 1 \ , \tag{A14}$$

which leads to the optimal weight set w_i^T for translation filters

$$w_i^T = N_T \frac{\langle \mu_i \rangle \sin \Theta_i}{\Delta t_i^2 + \Delta n_i^2} \ . \tag{A15}$$

For the plateau range model, we impose the condition that the filter output is 1 for some suitably chosen reference rotation or translation

$$\sum_{|\mathbf{u}_i \cdot \mathbf{p}_i| > P} w_i = 1 \tag{A16}$$

that results via the Euler–Lagrange equation

$$\frac{\partial}{\partial w_i} \left(\Delta e^2 - \lambda \left(\sum_{|\mathbf{u}_i \cdot \mathbf{p}_i| > P} w_i - 1 \right) \right) = 0 \ , \tag{A17}$$

in the optimal weight set

$$w_i = \frac{N \langle (\mathbf{u}_i \cdot \mathbf{p}_i)^2 \rangle}{\Delta t_i^2 + \Delta n_i^2} \tag{A18}$$

with N chosen such that (A16) is fulfilled.

In the case of a rotatory filter, the average squared flow projection during rotation about the filter axis is given by [cf.(A9) and (A1)]

$$\begin{aligned} \langle (\mathbf{u}_i \cdot \mathbf{p}_i)^2 \rangle &= \langle R^{\parallel 2} \rangle \sin^2 \Theta_i \\ &\quad + \langle \mu_i^2 \rangle \langle T_i^2 \rangle \ , \end{aligned} \tag{A19}$$

since $\mathbf{R}$ and $\mathbf{T}$ are assumed to be statistically independent. Similarly, we obtain for a translatory filter

$$\begin{aligned} \langle (\mathbf{u}_i \cdot \mathbf{p}_i)^2 \rangle &= \langle \mu_i^2 \rangle \langle T^{\parallel 2} \rangle \sin^2 \Theta_i \\ &\quad + \langle (\mathbf{d}_i \times \mathbf{R} \cdot \mathbf{u}_i)^2 \rangle \ . \end{aligned} \tag{A20}$$

Setting

$$r_i^2 = \frac{\langle (\mathbf{d}_i \times \mathbf{R} \cdot \mathbf{u}_i)^2 \rangle}{\langle T^{\parallel 2} \rangle} \tag{A21}$$

$$t_i^2 = \frac{\langle \mu_i^2 \rangle \langle T_i^2 \rangle}{\langle R^{\parallel 2} \rangle} \tag{A22}$$

and substituting these expressions in (A18) yields the weight sets of (9) and (10).

References

Allen C, Stevens CF (1994) An evaluation of causes for unreliability of synaptic transmission. Proc Natl Acad Sci USA 91: 10 380–10 383

Batschelet E (1981) Circular statistics in biology. Academic Press, London

Borst A, Egelhaaf M (1993) Detecting visual motion: theory and models. In: Miles FA, Wallman J (eds) Visual motion and its role in stabilization of gaze. Elsevier, Amsterdam, pp 3–27

Bouman MA, van de Grind WA, Zuidema P (1985) Quantum fluctuations in vision. In: Wolf E (ed) Progress in optics, vol XXII. North Holland, Amsterdam, pp 79–144

Bruss AR, Horn BKP (1983) Passive navigation. Comput Vision Graphics Image Process 21: 3–20

Buchner E (1976) Elementary movement detectors in an insect visual system. Biol Cybern 24: 85–101

Dahmen H, Wüst RW, Zeil J (1997) Extracting egomotion parameters from optic flow: principal limits for animals and machines. In: Srinivasan MV, Venkatesh S (eds) From living eyes to seeing machines. Oxford University Press, Oxford, pp 174–198

Egelhaaf M, Borst A (1993) Movement detection in arthropods. In: Miles FA, Wallman J (eds) Visual motion and its role in the stabilization of gaze. Elsevier, Amsterdam, pp 53–77

Franz MO, Neumann TR, Plagge M, Mallot HA, Zell A (1999) Can fly tangential neurons be used to estimate self-motion? In: Proceedings of the ninth international conference on artificial neural networks, ICANN 99. (IEE Conference Publication No. 470) London, pp 994–999

Götz KG, Hengstenberg B, Biesinger R (1979) Optomotor control of wing beat and body posture in *Drosophila*. Biol Cybern 35: 101–112

Hausen K (1982a) Motion sensitive interneurons in the optomotor system of the fly. I. The horizontal cells: structure and signals. Biol Cybern 45: 143–156

Hausen K (1982b) Motion sensitive interneurons in the optomotor system of the fly. II. The horizontal cells: receptive field organization and response characteristics. Biol Cybern 46: 67–79

Hausen K (1984) The lobula-complex of the fly: structure, function and significance in visual behaviour. In: Ali MA (ed) Photoreception and vision in invertebrates. Plenum Press, New York, pp 523–559

Hausen K (1993) The decoding of retinal image flow in insects. In: Miles FA, Wallman J (eds) Visual motion and its role in the stabilization of gaza. Elsevier, Amsterdam, pp 203–235

Hausen K, Egelhaaf M (1989) Neural M mechanisms of visual course control in insects. In: Stavenga DG, Hardie RC (eds) Facets of vision. Springer, Berlin Heidelberg New York, pp 391–424

Heeger DJ, Jepson AD (1992) Subspace methods for recovering rigid motion. I. Algorithm and implementation. Int J Comput Vision 7: 95–117

Hengstenberg R (1981) Rotatory visual responses of vertical cells in the lobula plate of *calliphora*. Verh Dtsch Zool Ges 74: 180

Hengstenberg R (1982) Common visual response properties of giant vertical cells in the lobula plate of the blowfly *Calliphora*. J Comp Physiol [A] 149: 179–193

Hengstenberg R, Hausen K, Hengstenberg B (1982) The number and structure of giant vertical cells (vs) in the lobula plate of the blowfly *Calliphora erythrocephala*. J Comp Physiol [A] 149: 163–177

Hildreth E (1992) Recovering heading for visually-guided navigation. Vision Res 32: 1177–1192

Koenderink JJ, van Doorn AJ (1987) Facts on optic flow. Biol Cybern 56: 247–254

Krapp HG, Hengstenberg R (1996) Estimation of self-motion by optic flow processing in single visual interneurons. Nature 384: 463–466

Krapp HG, Hengstenberg R (1997) A fast stimulus procedure to determine local receptive field properties of motion-sensitive visual interneurons. Vision Res 37: 225–234

Krapp HG, Hengstenberg B, Hengstenberg R (1998) Dendritic structure and receptive field organization of optic flow processing interneurons in the fly. J Neurophysiol 79: 1902–1917

Lappe M, Bremmer F, van den Berg AV (1999) Perception of self-motion from visual flow. Trends Cogn Sci 3(9): 329–336

Lappe M, Rauschecker JP (1993) A neural network for the processing of optic flow from egomotion in man and higher mammals. Neural Comp 5: 374–391

Longuet-Higgins HC, Prazdny K (1980) The interpretation of moving retinal images. Proc R Soc Lond B 208: 385–387

Nalbach H-O, Nalbach G (1987) Distribution of optokinetic sensitivity over the eye of crabs: its relation to habitat and possible role in flow-field analysis. J Comp Physiol [A] 160: 127–135

Perrone JA (1992) Model for the computation of self-motion in biological systems. J Opt Soc Am A 9: 177–194

Perrone JA, Stone LS (1994) A model of self-motion estimation within primate extrastriate visual cotrex. Vision Res 34: 2917–2938

Reichardt W (1987) Evaluation of optical motion information by movement detectors. J Comp Physiol [A] 161: 533–547

Reichardt W, Varjú D (1959) Vbertragvugseigenschaften im Auswertesystem für das Bewegingsschen. Z Naturforschng 14b: 674–689

Rieger JH, Lawton DT (1985) Processing differential image motion. J Opt Soc Am A 2: 354–360

Rosenfeld A, Kak AC (1982) Digital picture processing. Academic Press, London

Schilstra C, van Hateren JH (1998) Stabilizing gaze in flying blowflies. Nature 395: 654

Single S, Borst A (1998) Dendritic integration and its role in computing image velocity. Science 281(5384): 1848–1850

van Hateren JH (1990) Directional tuning curves, elementary movement detectors, and the estimation of the direction of visual movement. Vision Res 30(4): 603–614

Warzecha A-K, Egelhaaf M (1998) On the performance of biological movement detectors and ideal velocity sensors in the context of optomotor course stabilization. Vis Neurosci 15: 113–122

Wehner R (1987) Matched filters – neuronal models of the external world. J Comp Physiol [A] 161: 511–531